Engineering 25 (2023) 120–127

Contents lists available at ScienceDirect

Engineering

journal homepage: www.elsevier.com/locate/eng

Research
Biomedical Engineering—Article

Bio-Printed Hydrogel Textiles Based on Fish Skin Decellularized Extracellular Matrix for Wound Healing

Xiang Lin [a,b], Han Zhang [a], Hui Zhang [a], Zhuohao Zhang [a], Guopu Chen [a], Yuanjin Zhao [a,b,c,*]

[a] Department of Rheumatology and Immunology, Nanjing Drum Tower Hospital, School of Biological Science and Medical Engineering, Southeast University, Nanjing 210096, China
[b] Oujiang Laboratory (Zhejiang Lab for Regenerative Medicine, Vision, and Brain Health) & Wenzhou Institute, University of Chinese Academy of Sciences, Wenzhou 325001, China
[c] Chemistry and Biomedicine Innovation Center, Nanjing University, Nanjing 210023, China

ARTICLE INFO

Article history:
Received 7 December 2021
Revised 6 May 2022
Accepted 23 May 2022
Available online 19 May 2023

Keywords:
Bio-printing
Fish skin
Decellularized extracellular matrix
Hydrogel
Wound healing

ABSTRACT

Wound healing has always been a focus of clinical study due to its universality, difficult treatment, large number of patients, and heavy medical burden. A great deal of effort has been devoted to generating various wound dressings with special features and functions to satisfy specific demands. Here, we present novel bio-printed textiles based on fish skin decellularized extracellular matrix (dECM) for wound healing. Thanks to the desirable biocompatibility of the fish-derived dECM, the bio-printed textiles exhibit excellent performance in terms of cell adherence and proliferation. Since the dECM-based hydrogels are generated using a bio-printing method, the bio-printed textiles exhibit an adjustable porous structure with good air permeability throughout the whole textile. Moreover, the high specific surface areas of the porous structure on the hydrogel skeleton make it possible to load a variety of active molecules to improve the wound healing effect. According to an *in vivo* study, we demonstrate that the prepared textiles loaded with the active drug molecules curcumin (Cur) and basic fibroblast growth factor (bFGF) can significantly speed up the chronic wound healing process. These remarkable properties indicate the potential value of fish-skin-dECM textiles in wound healing and biomedical engineering.

1. Introduction

The skin is an important organ of the body that can perceive external stimuli, control body temperature, and prevent tissue fluid loss [1–3]. Extensive skin wounds can result from trauma, abrasions, skin ulceration, and burns; they are difficult to heal and may lead to further serious complications after bacterial infection. Consequently, wound healing has always been a basic issue of human health and an important direction of clinical research [4–8]. To achieve rapid wound healing, various biomedical materials including electrospun fibers, biofilms, porous sponges, and functional hydrogels have been developed [9–13]. Among them, hydrogels stand out due to their superior properties, which include maintaining a wet wound healing environment, reducing the wound surface temperature, promoting cell proliferation and migration, and promoting nutrient diffusion and penetration [14–16]. Many kinds of natural and synthetic polymers, including alginates (Alg), chitin, collagen, polylactic acid, and polyglycolic acid, have been used for fabricating functional hydrogel wound dressings [17–20]. Despite the many successes that have been achieved, most of the components of these materials are not easily available and require multiple chemical reactions or biological extractions. Furthermore, in order to generate wound dressings, most materials must be dissolved in toxic solvents and polymerized under extreme conditions, making the toxicity and biocompatibility of these materials a matter of concern [21–25]. Therefore, there is still an urgent demand for new polymer materials for fabricating functional wound dressings in the field of biomedicine.

In this paper, we propose a novel fish skin decellularized extracellular matrix (dECM) hydrogel textile with desirable features for wound healing, which is made using a bio-printing approach, as shown in Fig. 1. Materials based on dECM are considered to be promising due to their good histocompatibility, mechanical properties, and tissue cell induction function [26–28]. Compared with that in terrestrial animals, the collagen in fish skin has a unique biological activity due to its low thermal denaturation temperature, low thermal shrinkage, and low intermolecular

* Corresponding author.
E-mail address: yjzhao@seu.edu.cn (Y. Zhao).

https://doi.org/10.1016/j.eng.2022.05.022

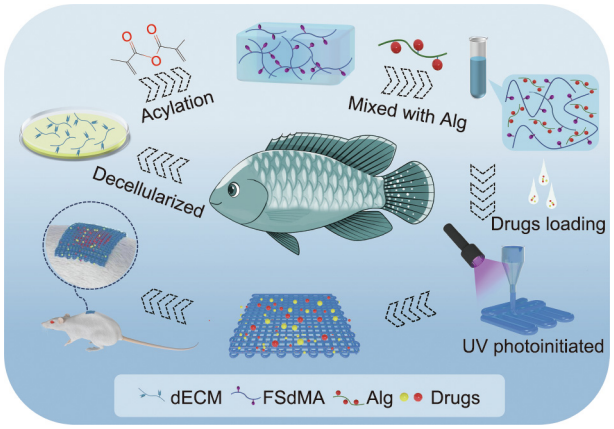

Fig. 1. Scheme of the fabrication and wound healing application of the bio-printed fish-skin-dECM methacrylate textiles. UV: ultraviolet; FSdMA: methacrylic anhydride (MA)-modified fish skin dECM.

cross-linking [29,30]. Thus, fish skin dECM has attracted great research interest within the field of biomedicine. However, most existing fish skin dECM hydrogels have simple structures and lack air permeability, which restricts many of their practical applications. As a burgeoning and versatile method for synthesizing functional materials, three-dimensional (3D) bio-printing technology can quickly and efficiently print 3D scaffolds with complex shapes or even personalized customization; it can also accurately regulate the porous structure of scaffolds at the micron scale [31–33]. Therefore, it is conceivable that the employment of 3D bio-printing for generating fish skin dECM textile as a novel functional wound dressing would provide a unique strategy for wound repair.

Herein, we report on the preparation of a kind of dECM from fish skin and its modification to obtain a photo-crosslinkable hydrogel. By employing a simple 3D bio-printing method to spin hydrogel microfibers and print them into 3D-structured textiles, we achieved a desirable textile for wound healing. It is worth mentioning that Alg was added to the dECM bio-ink due to its fast cross-linking and excellent rheological properties. With the high specific surface areas of the porous structure, it was possible to encapsulate the active pharmaceutical molecules curcumin (Cur) and basic fibroblast growth factor (bFGF) in the fish skin dECM textiles, where bFGF promotes the synthesis of elastic fibers and collagen around the wound, and Cur (extracted from turmeric) exhibits an inhibitory effect on inflammation, bacterial infection, and oxidant activity. Importantly, it was demonstrated that these fish skin dECM textiles showed excellent wound repair capabilities when treating cutaneous wounds in an infectious rat model. These characteristics indicate that the fish skin dECM textiles are ideal candidates for wound repair and other related biomedical fields.

2. Materials and methods

2.1. Materials

Fresh tilapia was purchased from Jinxianghe Road Market in Nanjing, China. Sodium alginate, pepsin, methacrylic anhydride (MA), sodium dodecyl sulfate (SDS), NaOH, rhodamine B (RhB, ≥95%, high performance liquid chromatography (HPLC) grade), 2-hydroxy-2-methylpropiophenone (HMPP), and dimethyl sulfoxide (DMSO) were obtained from Sigma-Aldrich, USA. SYTOX green (SYTO) and propidium iodide (PI) were obtained from Jiangsu KGI Biotechnology Co., Ltd. (China). Fluorescein isothiocyanate-labeled bovine serum albumin (FITC-BSA) was purchased from Zhongke Chenyang Technology Co., Ltd. (China). A Genomic DNA Extraction Kit was provided by TaKaRa Bio (Japan). NIH 3T3 cell lines were provided by the Chinese Academy of Sciences (Shanghai, China). Sprague–Dawley (SD) male rats between 200 and 220 g were purchased at Jinling Hospital (China). The rat experiments were performed after being reviewed by the Animal Investigation Ethics Committee of the Drum Tower Hospital (approval No.: 2021AE02018).

2.2. Characterization

The bio-printed process and pictures of the textiles were recorded in real time using a stereomicroscope (JSZ6S, Jiangnan Novel Optics, China). The morphology of the bio-printed hydrogel textiles was characterized using a field-emission scanning electron microscope (SEM, UltraPlus, Zeiss, Germany). A rheometer (MCR 302, Anton Paar, Austria) was used to measure the rheological properties of the pre-gel solution. For the nuclear magnetic resonance (NMR) test, samples were dissolved in D_2O and measured with an AVANCE III HD 600 MHz NMR spectrometer (Bruker, Germany). For the gel permeation chromatography (GPC) test (Agilent 1260, Agilent Technologies, Germany), samples were filtered through a microporous membrane (0.22 μm). Then, a 50 μL sample was taken for detection. The flow rate was 2 mL·min^{-1}, and the molecular weight distribution of the sample was determined by the elution time.

2.3. dECM extraction

The skin of the fish was cleaned and soaked in 0.5 mol·L^{-1} NaOH solution for 24 h. The bath ratio of the sample/alkaline solution was 1:40 (w/v), and a magnetic oscillator was used for stirring during the cleaning process. After that, the sample was decolorized using 3% H_2O_2 for 8 h. During the decolorization process, the sample/butanol ratio was 1:30 (w/v). Subsequently, a further decellularization process was conducted in a 10% (v/v) butanol solution with 2% SDS for 36 h. The decellularized fish skin was thoroughly cleaned and then freeze-dried. To extract the dECM, the freeze-dried residue was immersed in a solution containing 0.5% pepsin and 1 mol·L^{-1} acetic acid for 3 days, with the sample/solution ratio set to 1:50 (w/v). The dECM solution was then freeze-dried for further use.

2.4. DNA content

4′,6-Diamidino-2-phenylindole (DAPI) staining of the nuclei was conducted to evaluate the presence of residual nuclei on the surface of the fish skin. To further measure the DNA content, DNA was extracted from native fish skin and decellularized fish skin by means of a Genomic DNA Extraction Kit, and the extracted genomic DNA was quantified using a NanoDrop 8000 spectrophotometer (Thermo Fisher Scientific, USA).

2.5. Synthesis of MA-modified fish skin dECM (FSdMA)

A total of 2 g of dECM was placed into a beaker (with a rotor) with 100 mL of phosphate buffered saline (PBS)/10 mmol·L^{-1} HCl buffer and stirred at 4 °C until it was completely dissolved. Then, 0.2 mol·L^{-1} Na_2HPO_4 buffer was added until the pH reached 7.5. To graft the MA group, 5 mL of MA was gradually added in a drop-wise fashion to the above solution and stirred in an ice bath for 8 h away from light. When the solution system was stable, the remaining 150 mL of PBS buffer was added, and the mixture continued to react for 1–2 h. After the solution became clear again, the solution in the beaker was poured into a dialysis belt and immersed in ice water for more than 168 h. The water was changed three times a day, with the number of times the water was

changed being increased appropriately in the first 2 days. After dialysis, the liquid was poured into a container and freeze-dried.

2.6. Fabrication of FSdMA/Alg textiles

First, the printing platform was sterilized by means of ultraviolet (UV) light for 2 h. Then, a bio-printing platform (Bio-Architect, Regenovo, China) with longwave (365 nm) UV lamps was used to print the hydrogel textiles. To test the printability, different shapes of textiles were designed using 3D Studio Max, and all textiles were printed at room temperature. The synthesized FSdMA (15%) was mixed with a certain ratio of Alg (1%, 2%, 3%, or 5%) to form a pre-printed gel (containing 0.5% HMPP). All the mixed ink was well dissolved and left overnight before printing.

2.7. Drug-release properties of the textiles

For the drug-distribution and release kinetics analysis, RhB and FITC-BSA were selected. We dissolved each selected drug in the formulated ink to generate a hydrogel textile containing 1 mg·mL^{-1} RhB or 1 mg·mL^{-1} FITC-BSA. A fluorescence microscope was used to observe the effect of drug-distribution release at different time points. For the drug-release kinetics, 5 mg of drug-loaded hydrogel textile was immersed in 1 mL of PBS solution at 37 °C; in each testing cycle, 100 μL of the release medium was taken out and the same amount of PBS buffer was added.

A Cur-loaded hydrogel was prepared using a one-step solid dispersion method. In brief, Cur was dissolved in ethanol and then added to the formulated hydrogel solution with a final concentration of 1 mg·mL^{-1}; next, the solvent was removed by means of a rotary evaporator. The release process was conducted in PBS solution with Tween80 (0.5 wt%) at 37 °C. The released amounts of RhB and Cur were calculated according to the optical density (OD) value (Olympus, CKX41, Japan) of the released medium. The released amounts of FITC-BSA were measured by means of fluorescence intensity (Olympus, CKX41).

2.8. Antibacterial ability test

Escherichia coli (*E. coli*) and *Staphylococcus aureus* (*S. aureus*) were chosen to study the antibacterial ability of the Cur-loaded textiles. In brief, the turbidity of each bacterial suspension was controlled at about 0.5 (McFarland standard). Cur was mixed into 20% (w/v) FSdMA/Alg solution with a final concentration of 2, 3, or 4 mg·mL^{-1}. Cur-loaded hydrogel textiles with a dry weight of 5 mg were put into a 24-well plate with 1 mL of PBS buffer. Next, 100 μL of bacteria resuspension was dropped into each well and co-cultured for 24 h at 37 °C. Then, the solution was stained with SYTO9 and PI for 15 min, and 100 μL of the solution was taken out. Subsequently, the results were recorded using a fluorescence microscope.

2.9. Biocompatibility test

The 3T3 cells were separated into four groups with a cell density of 2×10^5 cells per milliliter per well in a 24-well plate (Thermo Fisher Scientific). After culturing for 72 h, 1.0 μL of Calcein-AM (Molecular Detector, Beyotime Biotechnology, China) was dropped into the culture medium to observe the living cells. For the 3-(4,5-dimethylthiazol-2-yl)-2,5-diphenyltetrazolium bromide (MTT) test, the cells were co-cultured with each group for 1, 2, or 3 days. The residual solution was removed before adding MTT solution. Next, the MTT solution (50 μL) was dropped into each group and the well-plate was co-cultured for another 4 h at 37 °C. The medium in each well was removed, and 600 μL of the DMSO was added to serve as a dissolving unit. The absorbance was obtained through a micro-plate reader (Olympus, CKX41).

2.10. Wound healing study

To evaluate the function of the hydrogel textiles in wound repair, a rat full-thickness infection wound model was created. Twenty-four healthy SD rats were separated into four groups. All the animals were anesthetized, and the hair on the dorsal surface was removed. A rat model of full-thickness skin infected defects was constructed by injecting 200 μL of *S. aureus* (10^8 colony-forming units (CFU) per milliliter) into a 1 cm-round wound. In the experimental groups, Cur and bFGF were loaded by means of an encapsulation method, with final respective concentrations of 3.0 and 0.1 mg·mL^{-1}. The four groups were treated with PBS (Group I), FSdMA/Alg textiles (Group II), Cur-loaded FSdMA/Alg textiles (Group III), and (Cur + bFGF)-loaded FSdMA/Alg textiles (Group IV), respectively. After that, all the animals were placed in separated cages. Optical images of the wounds were captured after 0, 3, 5, 7, and 9 days. The granulation tissues along with the surrounding tissues were isolated and stored in cold formaldehyde for further histology and immunohistochemistry analysis.

2.11. Statistical analysis

SPSSAU 24.0 was adopted to evaluate the statistical significance. The processed data was expressed as mean ± standard deviation. An independent-sample *t*-test was used to assess significant differences between the control group and experimental groups. $p < 0.05$ was selected as the significance level, where * represents $0.01 < p < 0.05$, and ** represents $p < 0.01$.

3. Results and discussion

In a typical experiment, tilapia fish skin was used as the raw material for generating the hydrogel textiles. First, the cleaned fish skin was successively treated with NaOH and SDS to remove unwanted cells and pigments; then, pepsin was used to extract dECM from the fish skin. The resultant product was freeze-dried for further use (Figs. S1(a)–(c) in Appendix A). Subsequently, a DNA content test was carried out to verify the effective removal of cells. The cellular residues in the decellularized fish skin were found to be less than 50 ng double-stranded DNA (dsDNA) per milligram, which made it possible to avoid immunological issues (Figs. S1(d)–(f) in Appendix A). To widen the application of the generated dECM, we modified the fish skin dECM with MA to obtain a kind of photo-crosslinkable hydrogel, as shown in Fig. S2 in Appendix A. Additional double peaks at 5–6 ppm according to the NMR spectroscopy results indicated the success of the MA modification (Figs. S3(a) and (b) in Appendix A). The molecular weight of the FSdMA indicated that the dECM primarily contained gelatin after collagen hydrolysis (Figs. S3(c) and (d) in Appendix A). However, the aqueous solution of the FSdMA generally exhibited a relatively low viscosity, which did not meet the requirements of bio-printing. Therefore, we added Alg to optimize the rheological properties of the FSdMA. As shown in Fig. S4(a) in Appendix A), it was found that the mixed pre-gel solution exhibited shear-thinning behavior as the shear rate increased. During the heating process from 5 to 45 °C, the viscosity of the FSdMA/Alg pre-gel solution increased significantly with an increase in the concentration of Alg (Fig. S4(b) in Appendix A). Moreover, the FSdMA/Alg pre-gel solution exhibited a gel form at room temperature, which helped maintain the morphology and structure of the printed hydrogel textile (Fig. S4(c) in Appendix A). These findings indicated that the mixed ink was suitable for bio-printing.

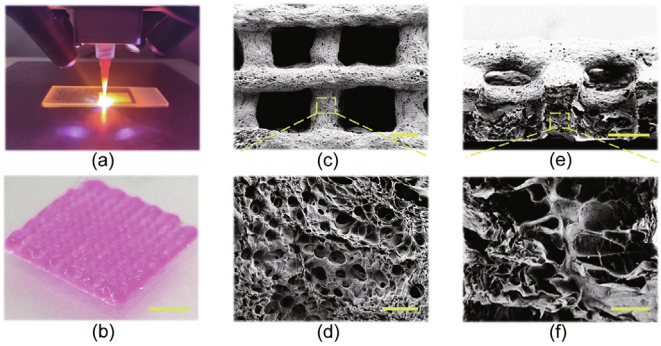

Fig. 2. (a) Digital image of printing textiles with the FSdMA/Alg pre-gel solution; (b) optical image of the bio-printed textile; (c–f) scanning electron microscopy (SEM) images of the FSdMA/Alg hydrogel textile at (c) the surface and (d) its magnified field, and (e) the cross-section and (f) its magnified field. Scale bars are 5 mm in part (b), 300 μm in parts (c) and (e), and 20 μm in parts (d) and (f).

After that, a modified 3D bio-printer, which included a syringe and four long-wave UV lamps, was used to generate the hydrogel textiles. The prepared FSdMA/Alg pre-gel solution was injected into an aluminum foil-wrapped syringe to prevent premature gelation; next, the mixed pre-gel solution was extruded through the syringe to fabricate the desired textiles, as shown in Fig. 2(a). By adjusting the extrusion speed of the pre-gel solution to match the movement speed of the syringe of the 3D printer, textiles with uniform morphology and 3D structure were generated after being irradiated with UV rays during the extrusion process (Figs. 2(b) and (c)). Moreover, increasing the Alg concentration significantly increased the ink viscosity, ensuring that the extruded filaments had a smooth surface to enhance the accuracy of the printing process.

To increase the accuracy of the printed textile, we chose to use a mixed gel with a ratio of 15% FSdMA and 5% Alg in the subsequent experiments (Fig. S5 in Appendix A). In order to print high-quality FSdMA/Alg hydrogel textiles, we first studied the printability under different printing parameters. Obviously, the use of a larger nozzle diameter resulted in a larger diameter of the printing fiber, *D*, as shown in Fig. S6(a) in Appendix A. It was notable that, due to the expansion effect of the viscoelastic pre-gel solution, the diameter of the extruded fiber was larger than the nozzle diameter. Studies have indicated that a larger extrusion force produces a more obvious mold expansion effect, resulting in an increase in the printing fiber diameter *D* with increasing pressure (Fig. S6(b) in Appendix A). Furthermore, the distance between the fibers and the cross angle of the fibers could be changed to adjust the morphology of the pores (Fig. S7 in Appendix A). These printing settings could be used to effectively control the bio-printed fiber diameter *D* and the pore length. Moreover, the slice shape of the 3D model could be changed to obtain textiles with different shapes (Fig. S8 in Appendix A).

In addition, the microstructures of the FSdMA/Alg hydrogel textiles were characterized, and it was found that the generated textiles had a porous, rough surface (Figs. 2(d) and (e)). The bio-printed FSdMA/Alg hydrogel textiles also exhibited interconnected internal pores after being freeze-dried (Fig. 2(f)). These unique microstructures of the FSdMA/Alg hydrogel textiles provide potential for drug loading and release.

Due to the porous surfaces and interconnected internal pores, the hydrogel textiles have huge specific surfaces areas, plenty of nano-pores, and intricate nanochannels to load many biological actives. Therefore, it is conceivable that the FSdMA/Alg textiles could be used as a sustained-release scaffold for containing active reagents. To evaluate this capability, we first selected RhB and FITC-BSA for characterizing the textiles' drug-release performance with a small-molecule drug and a proteinic drug, respectively. Drug loading was performed by means of encapsulation. The fluorescence images showed that both drugs could be completely and uniformly distributed in the textile and then released over time, indicating that the drug loading was successful (Figs. 3(a) and (b)).

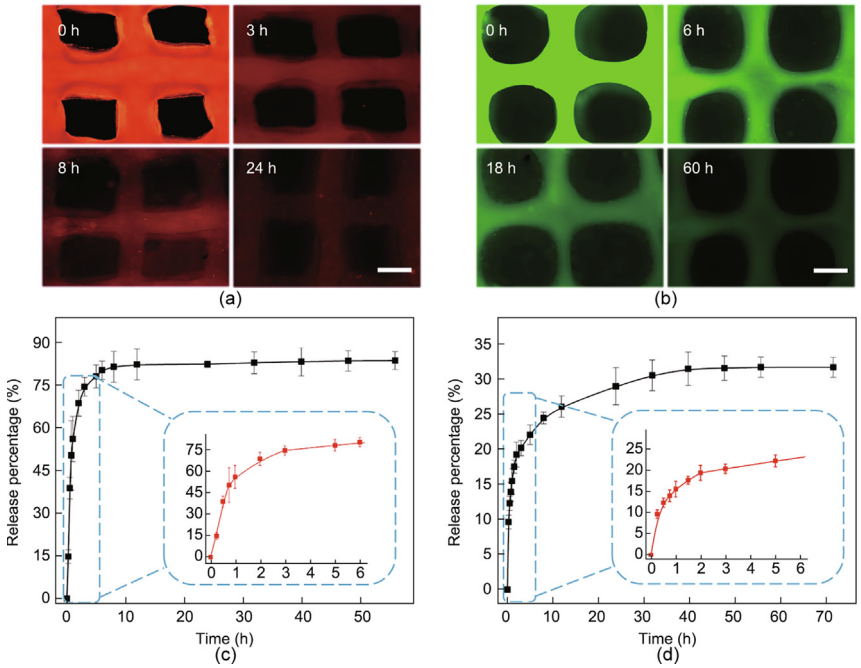

Fig. 3. (a) Fluorescence images of the RhB-loaded hydrogel textiles after 0, 3, 8, and 24 h; (b) fluorescence images of the FITC-BSA-loaded hydrogel textiles after 0, 6, 18, and 60 h; (c) release condition of the RhB-loaded textiles in PBS solution, where the lower right curve is that within 6 h ($n = 4$); (d) release condition of the FITC-BSA-loaded textiles in PBS solution, where the lower right curve is that within 6 h ($n = 4$). Error bar represents standard deviation. Scale bars are 400 μm in parts (a) and (b).

We also investigated the release kinetics of the small-molecule drug and proteinic drug (Figs. 3(c) and (d)). The standard curves are recorded in Figs. S9(a) and (b) in Appendix A. It was observed that the small-molecule drug RhB had a fast release in the first 6 h, followed by a sustained release process that lasted up to 12 h. Equilibrium was then gradually reached in 24 h. For the textiles loaded with FITC-BSA, it was apparent that the release process was slower than that of the RhB-loaded textiles, due to the large molecular weight of the proteinic drug. In addition, the release percentage of the RhB textiles was higher than that of the FITC-BSA-loaded textiles, which was because the small-molecule drug was more likely to escape through the small internal pores and channels of the textiles. Therefore, the bio-printed hydrogel textiles could be loaded with drugs with different molecular weights to serve various purposes.

Based on these features, we designed a novel antibacterial textile loading with Cur. We found that Cur exhibits anti-microbial properties against many microorganisms by inhibiting the formation of bacterial biofilms and can be used to treat infectious bacterial diseases. We also found that, as a small-molecule drug, the Cur had a slower release process than the RhB, which could be attributed to the difference in hydrophilicity (Figs. S9(c) and (d) in Appendix A). Notably, it was difficult to dissolve Cur in water, although it could be well-dispersed in polymeric micelles (Fig. S10 in Appendix A).

To evaluate the potential impact of the Cur-loaded textiles' *in vitro* antibacterial ability, we chose FSdMA/Alg textiles with different Cur loading concentrations as the bacterial growth substrate, respectively, and used two different types of bacteria (*E. coli* and *S. aureus*) for the investigation. Fluorescent images of live and dead bacteria and statistical analyses of the bacteria viabilities in different groups are provided in Figs. 4(a)–(e). It was found that, compared with the control group, the groups of Cur-loaded FSdMA/Alg textiles had a greater quantity of dead bacteria, for both kinds of bacteria. In addition, by increasing the concentration, the Cur-loaded textiles had a more significant antibacterial effect on *S. aureus*. This finding may be attributed to the difference in biofilm constituents and structure between *E. coli* and *S. aureus*. In particular, when the concentration of Cur in pre-gel solution was increased to 3 mg·mL^{-1}, up to 90% of the living *S. aureus* were killed. As Cur is a biologically active drug, an increased concentration of Cur would affect the biocompatibility of materials for biomedical applications. Therefore, the appropriate concentration of Cur was set at 3 mg·mL^{-1}.

Before exploring the practical application value of the generated drug-loaded textiles *in vivo*, their biocompatibility was studied.

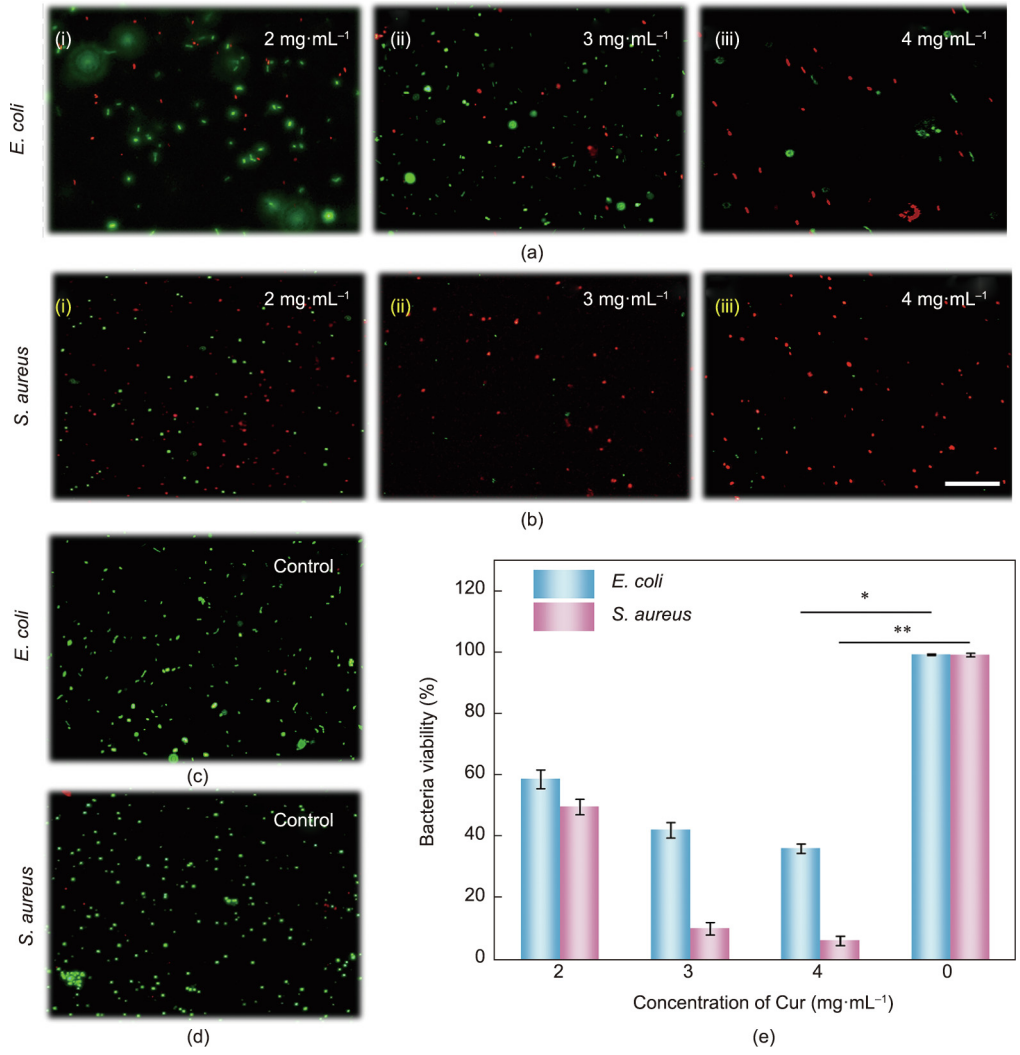

Fig. 4. (a, b) Live/dead staining of (a) *E. coli* and (b) *S. aureus* co-cultured with Cur-loaded FSdMA/Alg textiles: (i) 2 mg·mL^{-1} Cur; (ii) 3 mg·mL^{-1} Cur; and (iii) 4 mg·mL^{-1} Cur. (c, d) PBS against (c) *E. coli* and (d) *S. aureus*. (e) Statistical image of the viability of different groups. $n = 5$ for each group; error bar represents standard deviation. $^{*}p < 0.05$, $^{**}p < 0.01$. Scale bar is 50 μm.

From the fluorescence microscope images (Fig. S11(a) in Appendix A), it was found that the 3T3 cells in all groups showed good morphology after 3 days, indicating the excellent biocompatibility of the FSdMA and mixed hydrogel. Furthermore, to quantitatively study the cell viability of cells in different groups, an MTT assay was conducted (Fig. S11(b) in Appendix A), and the results were found to be consistent with the fluorescence pictures. These findings demonstrated the feasibility of the *in vivo* application of the FSdMA/Alg hydrogel.

Furthermore, we conducted *in vivo* experiments to evaluate the potential of the FSdMA/Alg textiles for wound healing (Fig. 5). In addition to textiles with antibacterial properties, hydrogel textiles incorporating both Cur and bFGF—the latter of which can promote the proliferation of multiple cell types—were used in experiments to improve the wound repair process. The test samples were divided into four groups: wound washed with PBS only (Group I); wound treated with FSdMA/Alg textiles (Group II); wound treated with Cur-loaded FSdMA/Alg textiles (Group III); and wound treated with (Cur + bFGF)-loaded FSdMA/Alg textiles (Group IV). The wound closure conditions during the wound healing process were recorded for a detailed analysis (Figs. 5(a) and (c)). It was found that, under the action of Cur + bFGF, Group IV showed the best closure rate, while the wounds in Group I healed relatively slowly. In order to further explore the wound healing conditions, hematoxylin–eosin (H&E) staining was used to observe the regenerated granulation tissue (Fig. 5(b)). The granulation tissue thicknesses of Groups I, II, III, and IV on Day 9 were (1.05 ± 0.16), (1.50 ± 0.10), (1.64 ± 0.09), and (2.02 ± 0.17) mm, respectively (Fig. 5(d)). Compared with Group I, the granulation tissue thickness was improved in the two groups with different types of drug-loaded functional FSdMA/Alg hydrogel textiles (Groups III and IV). These results indicate the improved wound healing efficiency of the drug-loaded groups.

Immunohistochemical (IHC) staining for tumor necrosis factor alpha (TNF-α), cluster of differentiation 31 (CD31), and interleukin 6 (IL-6) was respectively performed to evaluate inflammation and angiogenesis (Fig. 6). Wound infection is the main cause of chronic wounds, so the efficacy of the Cur-loaded textiles in preventing infection was studied through TNF-α and IL-6. In Group IV, IHC staining showed little sign of inflammation or infection with a low level of TNF-α and IL-6 secretion, which indicated lower immune reaction after being treated with drug-loaded FSdMA/Alg textiles. In contrast, large quantities of TNF-α and IL-6 were observed in Group I (Fig. 6(a); Fig. S12 in Appendix A). In addition, in the final stage of wound healing and remodeling, collagen is deposited as a skin component of the wound bed. The degree of directional arrangement and collagen deposition of Group IV indicated the good performance of the functionalized FSdMA/Alg

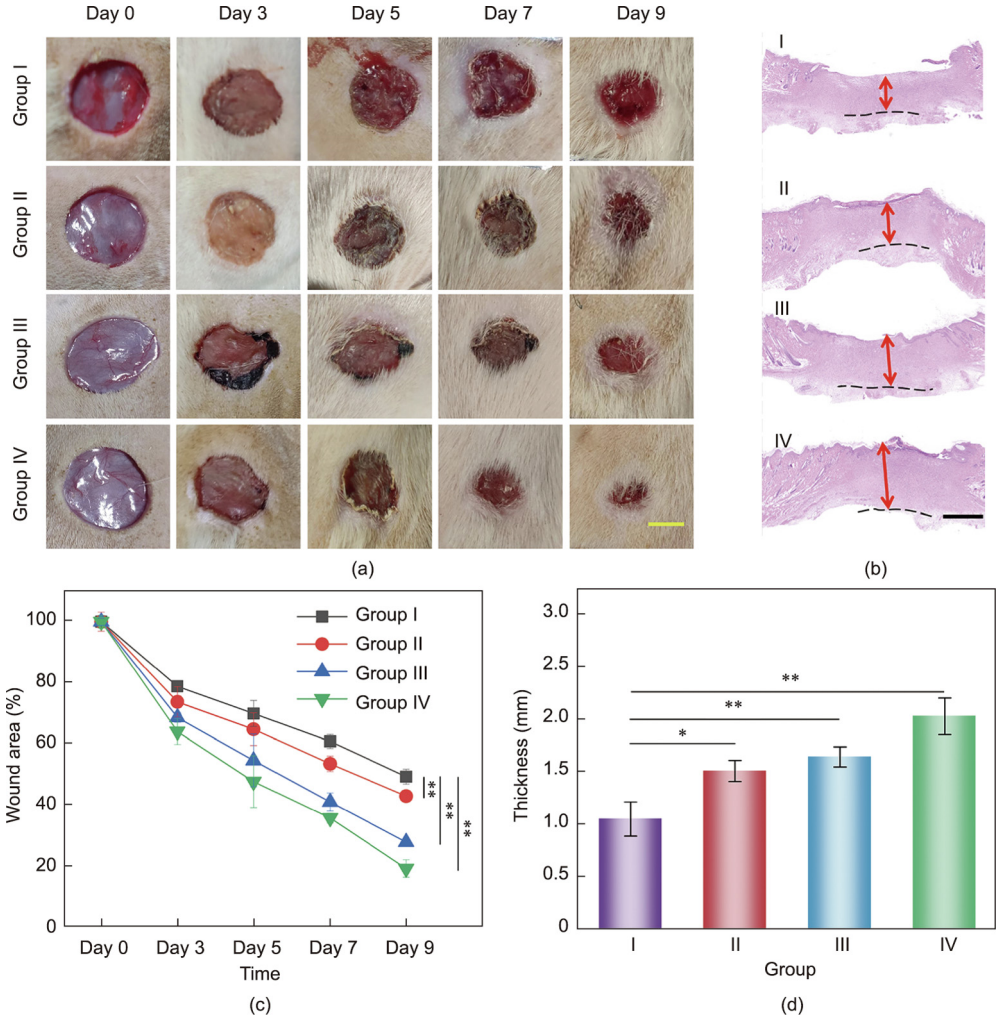

Fig. 5. (a) Representative images of tissue defects on Day 0, 3, 5, 7, and 9; (b) hematoxylin–eosin staining of isolated tissues after 9 days (dotted line and arrow indicate the boundaries of granulation tissue and their thickness, respectively; I–IV represent Groups I–IV, respectively); (c) quantification of the wound area on Day 0, 3, 5, 7, and 9; (d) quantification of the granulated tissue thickness after 9 days. $n = 3$ for each group; error bar represents the standard deviation. $^{*}p < 0.05$, $^{**}p < 0.01$. Scale bars are 5 mm in part (a) and 500 μm in part (b).

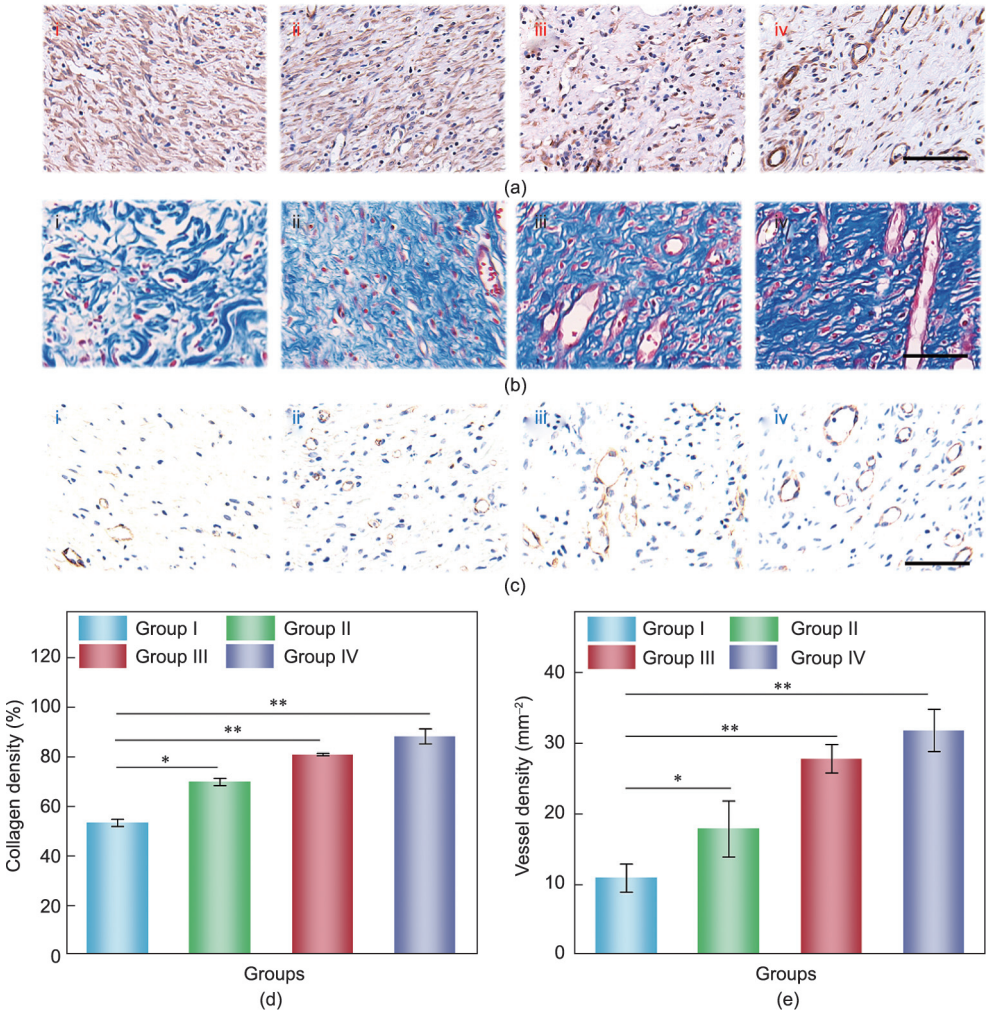

Fig. 6. (a) Immunohistochemistry staining of TNF-α after 9 days; (b) Masson-stained images of granulation tissues after 9 days; (c) CD31 staining of granulation tissues after 9 days; (d) quantification of collagen density after 9 days; (e) quantification of density of blood vessel. $n = 3$ for each group; error bar represents the standard deviation. $^{*}p < 0.05$, $^{**}p < 0.01$. i–iv in (a–c) represent Groups I–IV, respectively; scale bars in (a–c) are all 100 μm.

textiles in wound healing (Figs. 6(b) and (d)). Activation of neovascularization promoted the formation of regenerative tissues, which provide adequate nutrition and oxygen and promote the transport of cytokines and cell migration. As shown in Figs. 6(c) and (e), it was also observed that the number of newly formed blood vessels was significantly greater in Group IV compared with Group I. This result could be attributed to the presence of bFGF, which can promote neovascularization. In addition, vascular structures were present at a moderate level in Groups II and III. These results demonstrate the excellent functions of the drug-loaded FSdMA/Alg hydrogel textiles in angiogenesis.

4. Conclusions

In summary, we proposed a kind of dECM from fish skin and modified it to obtain a functional FSdMA hydrogel. The fish skin dECM was extracted using pepsin; it was then acylated with MA and mixed with Alg to obtain a mixed solution with good printable properties. By adjusting the printing parameters, such as the slice shape, pinhole diameter, and air pressure, the shape of the porous scaffold and the diameter of a single fiber could be controlled. In addition, by loading the antibacterial drug Cur and the growth factor bFGF, the textile was endowed with antibacterial properties and growth-promoting properties, making it better able to inhibit the growth of bacteria, promote cell proliferation, and accelerate wound healing. The FSdMA/Alg hydrogel textiles exhibited satisfactory therapeutic effects when used to treat SD rats with bacterial infection and injury. Thus, the abovementioned features give the proposed hydrogel textiles practical value for wound healing in a clinical setting.

Acknowledgments

This work was supported by the National Key Research and Development Program of China (2020YFA0908200), the National Natural Science Foundation of China (T2225003 and 52073060), the Nanjing Medical Science and Technique Development Foundation (ZKX21019), the Clinical Trials from Nanjing Drum Tower Hospital (2022-LCYJ-ZD-01), Guangdong Basic and Applied Basic Research Foundation (2021B1515120054), and the Shenzhen Fundamental Research Program (JCYJ20190813152616459 and JCYJ20210324133214038).

Authors' contributions

Yuanjin Zhao conceived the idea and designed the experiment. Xiang Lin conducted experiments and data analysis. Han Zhang and Hui Zhang assisted with data analysis and paper writing. Zhuohao Zhang and Guopu Chen contributed to the scientific discussion of the article. Xiang Lin and Yuanjin Zhao wrote the manuscript.

Compliance with ethics guidelines

Xiang Lin, Han Zhang, Hui Zhang, Zhuohao Zhang, Guopu Chen, and Yuanjin Zhao declare that they have no conflict of interest or financial conflicts to disclose.

Appendix A. Supplementary data

Supplementary data to this article can be found online at https://doi.org/10.1016/j.eng.2022.05.022.

References

[1] Zhou F, Hong Y, Liang R, Zhang X, Liao Y, Jiang D, et al. Rapid printing of bio-inspired 3D tissue constructs for skin regeneration. Biomaterials 2020;258:120287.
[2] Correa-Gallegos D, Jiang D, Christ S, Ramesh P, Ye H, Wannemacher J, et al. Patch repair of deep wounds by mobilized fascia. Nature 2019;576(7786):287–92.
[3] Kurita M, Araoka T, Hishida T, O'Keefe DD, Takahashi Y, Sakamoto A, et al. *In vivo* reprogramming of wound-resident cells generates skin epithelial tissue. Nature 2018;561(7722):243–7.
[4] Zhao X, Liang Y, Huang Y, He J, Han Y, Guo B. Physical double-network hydrogel adhesives with rapid shape adaptability, fast self-healing, antioxidant and NIR/pH stimulus-responsiveness for multidrug-resistant bacterial infection and removable wound dressing. Adv Funct Mater 2020;30(17):1910748.
[5] Zhao Y, Li Z, Song S, Yang K, Liu H, Yang Z, et al. Skin-inspired antibacterial conductive hydrogels for epidermal sensors and diabetic foot wound dressings. Adv Funct Mater 2019;29(31):1901474.
[6] Pang Q, Lou D, Li S, Wang G, Qiao B, Dong S, et al. Smart flexible electronics-integrated wound dressing for real-time monitoring and on-demand treatment of infected wounds. Adv Sci 2020;7(6):1902673.
[7] Liang Y, Chen B, Li M, He J, Yin Z, Guo B. Injectable antimicrobial conductive hydrogels for wound disinfection and infectious wound healing. Biomacromolecules 2020;21(5):1841–52.
[8] Gao G, Jiang YW, Jia HR, Wu FG. Near-infrared light-controllable on-demand antibiotics release using thermo-sensitive hydrogel-based drug reservoir for combating bacterial infection. Biomaterials 2019;188:83–95.
[9] Cheng H, Shi Z, Yue K, Huang X, Xu Y, Gao C, et al. Sprayable hydrogel dressing accelerates wound healing with combined reactive oxygen species-scavenging and antibacterial abilities. Acta Biomater 2021;124:219–32.
[10] Yao X, Zhu G, Zhu P, Ma J, Chen W, Liu Z, et al. Omniphobic ZIF-8@hydrogel membrane by microfluidic-emulsion-templating method for wound healing. Adv Funct Mater 2020;30(13):1909389.
[11] Qu J, Zhao X, Liang Y, Xu Y, Ma PX, Guo B. Degradable conductive injectable hydrogels as novel antibacterial, anti-oxidant wound dressings for wound healing. Chem Eng J 2019;362:548–60.
[12] Yang J, Wang K, Yu DG, Yang Y, Bligh SWA, Williams GR. Electrospun Janus nanofibers loaded with a drug and inorganic nanoparticles as an effective antibacterial wound dressing. Mater Sci Eng C 2020;111:110805.
[13] Zhang XX, Chen GP, Yu YR, Sun LY, Zhao YJ. Bioinspired adhesive and antibacterial microneedles for versatile transdermal drug delivery. Research 2020;2020:3672120.
[14] Wang C, Lai J, Li K, Zhu S, Lu B, Liu J, et al. Cryogenic 3D printing of dual-delivery scaffolds for improved bone regeneration with enhanced vascularization. Bioact Mater 2021;6(1):137–45.
[15] Qiao Z, Lian M, Han Y, Sun B, Zhang X, Jiang W, et al. Bioinspired stratified electrowritten fiber-reinforced hydrogel constructs with layer-specific induction capacity for functional osteochondral regeneration. Biomaterials 2021;266:120385.
[16] Chaudhuri O, Cooper-White J, Janmey PA, Mooney DJ, Shenoy VB. Effects of extracellular matrix viscoelasticity on cellular behaviour. Nature 2020;584(7822):535–46.
[17] Mao X, Cheng R, Zhang H, Bae J, Cheng L, Zhang L, et al. Self-healing and injectable hydrogel for matching skin flap regeneration. Adv Sci 2019;6(13):1901124.
[18] Hamad K, Kaseem M, Yang HW, Deri F, Ko YG. Properties and medical applications of polylactic acid: a review. Express Polym Lett 2015;9(5):435–55.
[19] Mogoşanu GD, Grumezescu AM. Natural and synthetic polymers for wounds and burns dressing. Int J Pharm 2014;463(2):127–36.
[20] Bagher Z, Ehterami A, Safdel MH, Khastar H, Semiari H, Asefnejad A, et al. Wound healing with alginate/chitosan hydrogel containing hesperidin in rat model. J Drug Deliv Sci Technol 2020;55:101379.
[21] Chen X, Villa NS, Zhuang YF, Chen LZ, Wang TF, Li ZD, et al. Stretchable supercapacitors as emergent energy storage units for health monitoring bioelectronics. Adv Energy Mater 2020;10(4):1902769.
[22] Zhang H, Chen G, Yu Y, Guo J, Tan Q, Zhao Y. Microfluidic printing of slippery textiles for medical drainage around wounds. Adv Sci 2020;7(16):2000789.
[23] Ghavami Nejad A, Park CH, Kim CS. *In situ* synthesis of antimicrobial silver nanoparticles within antifouling zwitterionic hydrogels by catecholic redox chemistry for wound healing application. Biomacromolecules 2016;17(3):1213–23.
[24] Gupta A, Briffa SM, Swingler S, Gibson H, Kannappan V, Adamus G, et al. Synthesis of silver nanoparticles using curcumin-cyclodextrins loaded into bacterial cellulose-based hydrogels for wound dressing applications. Biomacromolecules 2020;21(5):1802–11.
[25] Yang K, Han Q, Chen B, Zheng Y, Zhang K, Li Q, et al. Antimicrobial hydrogels: promising materials for medical application. Int J Nanomedicine 2018;13:2217–63.
[26] Kim BS, Lee JS, Gao G, Cho DW. Direct 3D cell-printing of human skin with functional transwell system. Biofabrication 2017;9(2):025034.
[27] Crapo PM, Gilbert TW, Badylak SF. An overview of tissue and whole organ decellularization processes. Biomaterials 2011;32(12):3233–43.
[28] Karimi A, Navidbakhsh M. Material properties in unconfined compression of gelatin hydrogel for skin tissue engineering applications. Biomed Eng/Biomed Te 2014;59(6):479–86.
[29] Subhan F, Hussain Z, Tauseef I, Shehzad A, Wahid F. A review on recent advances and applications of fish collagen. Crit Rev Food Sci Nutr 2021;61(6):1027–37.
[30] Chen J, Gao K, Liu S, Wang S, Elango J, Bao B, et al. Fish collagen surgical compress repairing characteristics on wound healing process *in vivo*. Mar Drugs 2019;17(1):33.
[31] Yang Q, Li H, Li M, Li Y, Chen S, Bao B, et al. Rayleigh instability-assisted satellite droplets elimination in inkjet printing. ACS Appl Mater Interfaces 2017;9(47):41521–8.
[32] Luo Y, Wei X, Wan Y, Lin X, Wang Z, Huang P. 3D printing of hydrogel scaffolds for future application in photothermal therapy of breast cancer and tissue repair. Acta Biomater 2019;92:37–47.
[33] De Santis MM, Alsafadi HN, Tas S, Bölükbas DA, Prithiviraj S, Da Silva IAN, et al. Extracellular-matrix-reinforced bioinks for 3D bioprinting human tissue. Adv Mater 2021;33(3):2005476.